

Self-assembly and dynamic behavior of colloidal rods in the isotropic phase

Md. Arif Kamal,¹ Thomas Zinn^{2,*} and Antara Pal^{3,4,†}

¹*Division of Physical Chemistry, Department of Chemistry, Lund University, Lund, Sweden*

²*ESRF—The European Synchrotron, Grenoble, France*

³*Department of Biomedical Science, Malmö University, Malmö, Sweden*

⁴*Biofilms Research Center for Biointerfaces, Malmö University, Malmö, Sweden*



(Received 10 October 2025; accepted 4 March 2026; published 31 March 2026)

In this study, we have investigated the dynamic behavior of colloidal rods within their isotropic phase, employing multispeckle ultrasmall-angle x-ray photon correlation spectroscopy (UA-XPCS) focusing on the understanding of the interplay between structure and dynamics at the nearest-neighbor length scale. While prior research has primarily focused on the structural aspects, our work addresses the lesser-explored realm of dynamic behavior. Through ultrasmall-angle x-ray scattering and UA-XPCS, we have measured the key parameters, such as the effective structure factor ($S_{\text{eff}}(q)$) and the effective diffusion coefficient ($D_{\text{eff}}(q)$). A significant finding is the scaling relationship between $D_{\text{eff}}(q)$ and $1/S_{\text{eff}}(q)$, implying a connection between particle diffusion and structural arrangement. Additionally, the estimated scaling parameter (effective amplitude function, $A_{\text{eff}}(q)$), which can be directly related to the effective hydrodynamic function ($H_{\text{eff}}(q)$) shows a similar dependence on wave vector (q) as $S_{\text{eff}}(q)$. Furthermore, our study precisely determines the volume fraction at which the arrest transition occurs. These findings shed light on the influence of structures on the intricate dynamics of anisotropic colloidal systems.

DOI: [10.1103/5cbx-gnc4](https://doi.org/10.1103/5cbx-gnc4)

I. INTRODUCTION

Anisotropic colloids can be broadly categorized into systems composed of aspherical particles, low-aspect-ratio ellipsoids, low-aspect-ratio rods, and high-aspect-ratio rods. Each of these classes exhibits distinct structural and dynamical behavior, driven by differences in rotational-translational coupling, excluded-volume interactions, and the degree of entanglement. At sufficiently high concentrations, long rods enter an entangled regime in which rotational diffusion becomes strongly suppressed and is effectively captured by Doi-Edwards-type tubelike confinement models [1]. In contrast, shorter rods or weakly anisotropic particles do not experience the same level of topological constraints and are instead more accurately described by glasslike caging behavior or the dynamics characteristic of dense suspensions [2].

Despite this diversity in behavior, most existing studies have focused primarily on structural properties, leaving the dynamic response of anisotropic particles comparatively less explored. Among the best-studied systems are colloidal

ellipsoids and rods [3–8], though these investigations rely largely on particle-tracking methods and are therefore restricted to quasi-two-dimensional (quasi-2D) geometries. In bulk suspensions, polarized and depolarized light-scattering techniques have been used to extract average translational and rotational diffusion coefficients for various anisotropic particles [9–13]. However, strong multiple scattering at high concentrations renders such measurements extremely challenging, limiting most bulk studies to the dilute regime. As a result, a systematic understanding of how structure and dynamics evolve near ordered phases or the arrested, glassy state remains incomplete, with only a few notable exceptions [13–17].

Depending on the interaction potential, suspensions of rods can form microstructures ranging from heterogeneous fractal clusters to homogeneous fiber networks. Theories of Brownian dynamics predict that these distinct microstructural motifs lead to different routes to dynamical arrest—gelation in the case of fractal clusters and glasslike slowing down for fiber networks. The volume-fraction and aspect-ratio dependences of the resulting dynamics therefore differ substantially. Although considerable effort has been devoted to understanding the rheology of the dispersions of rods across a range of aspect ratios, concentrations, and material systems, the connection between microstructure and dynamics remains incomplete, particularly at high concentrations [18]. Advancing this understanding is essential not only from a fundamental perspective but also for optimizing the performance of rod-based materials in technological applications.

Rodlike colloids are abundant in nature, spanning biological filaments such as F-actin and fd virus, inorganic systems

*Present address: Diamond Light Source Ltd., Didcot, United Kingdom.

†Contact author: antara.pal@mau.se

Published by the American Physical Society under the terms of the [Creative Commons Attribution 4.0 International license](https://creativecommons.org/licenses/by/4.0/). Further distribution of this work must maintain attribution to the author(s) and the published article's title, journal citation, and DOI. Funded by [Bibsam](https://www.bibsam.org/).

including boehmite and hematite, and commercial fibers such as cellulose ([18] and references therein). Especially for biological rod systems such as fd virus, extensive work has shown that both rod length and aspect ratio strongly influence the slowing down of the dynamics. Recent microscopy-based studies have further revealed that the dynamics can be highly heterogeneous, involving intermittent reorientation events and abrupt angular changes—highlighting that single-particle behavior can be significantly richer than what is accessible through ensemble-averaged scattering measurements [1,19].

A key experimental challenge is that different techniques provide complementary yet incomplete information. Microscopy-based particle tracking offers direct access to single-particle trajectories and can reveal complex heterogeneous dynamics, but extracting quantitative bulk structural information from microscopy becomes extremely difficult in dense suspensions. Scattering techniques, in contrast, provide ensemble-averaged structural and dynamical information simultaneously, which is crucial for establishing quantitative structure-dynamics relations in concentrated systems.

In recent years, synchrotron-based multispeckle x-ray photon correlation spectroscopy (XPCS) has emerged as a powerful alternative for probing dynamics at colloidal length scales [15,16,20–26]. While XPCS is conceptually analogous to dynamic light scattering (DLS), the use of X-rays circumvents the multiple-scattering and absorption issues that limit DLS in opaque or highly concentrated suspensions of inorganic particles. Earlier scattering studies on rodlike viruses such as fd virus have demonstrated that light scattering can yield valuable insights into rod dynamics when samples remain optically accessible [27]. However, many technologically relevant rod systems consist of shorter rods and/or are studied at much higher concentrations, where multiple scattering and opacity preclude the use of conventional DLS. In this regime, XPCS provides a unique opportunity to probe bulk dynamics in dense suspensions of short rods.

Despite this potential, most XPCS studies of colloidal dynamics have focused on spherical particles [22–24], with only a few investigations addressing anisotropic systems [17,20,28,29]. The presence of anisotropy—both in particle shape and in interaction potentials—introduces additional complexity in the resulting self-assembled structures and their dynamics, underscoring the need for systematic studies on rodlike colloids.

We report a detailed experimental investigation of the dynamics of colloidal akaganeite rods (aspect ratio $\rho = 7.2$) across a range of volume fractions (ϕ) in the isotropic phase. We focus on the intermediate regime lying between classical long-rod entangled systems and weakly anisotropic particle suspensions. Although the dynamics of very slender rods ($L/D \gg 1$) at high concentrations are well described by entanglement-based theories such as the Doi-Edwards framework—where each rod is effectively confined within a tube formed by its neighbors—these asymptotic descriptions do not straightforwardly apply to rods of moderate aspect ratio. In the entangled limit, rotational diffusion is strongly suppressed and relaxation proceeds primarily through reptationlike motion along the rod axis.

For rods of moderate aspect ratio, such as those studied here ($L/D \approx 7.2$), it is not evident *a priori* whether the

dominant mechanism of dynamical slowing down arises from entanglement physics, glasslike caging, or microstructure-controlled constraints. The geometric restrictions are weaker, topological entanglement is less pronounced, and rotational and translational degrees of freedom remain strongly coupled. As a result, the slowing down of dynamics in this regime reflects a combination of steric crowding, transient caging, and local microstructural organization rather than tubelike confinement alone.

By combining XPCS measurements of dynamics with simultaneous structural characterization, we are able to directly probe this intermediate regime and clarify how microstructure governs the slowing down of motion in dense suspensions of short anisotropic rods. This integrated approach allows us to move beyond the limiting cases of tubelike entanglement and simple caging, and to establish quantitative links between the local organization of the rods and their collective relaxation behavior. Across all concentrations studied, the density fluctuations relax through a single decay process, from which we extract the effective diffusion coefficient $D_{\text{eff}}(q)$. We find that $D_{\text{eff}}(q)$ scales inversely with the effective structure factor $S_{\text{eff}}(q)$ for all ϕ , enabling us to define an effective amplitude function $A_{\text{eff}}(q)$, analogous to the effective hydrodynamic function $H_{\text{eff}}(q)$ that governs the scaling of the pure short-time diffusion coefficient $D_{\text{eff}}^s(q)$ with $1/S_{\text{eff}}(q)$ [30–35]. Using this scaling, we determine $A_{\text{eff}}(q)$ for colloidal rods with $\rho = 7.2$ and find that its q dependence closely mirrors that of $S_{\text{eff}}(q)$. Both the structural correlations and the diffusion coefficients are isotropic, consistent with previous observations in colloidal ellipsoids [15,16]. The evolution of $D_{\text{eff}}(q)$ with increasing ϕ further indicates that the system approaches a kinetically arrested state at $\phi_m = 0.23$. Finally, we attempt to separate translational and rotational contributions following the model of Dhont [36], although its assumptions of infinitely thin rods under infinite dilution limit its applicability to the present system.

II. EXPERIMENTAL SECTION

A. Synthesis

Reagent grade ferric chloride hexahydrate was purchased from Sigma-Aldrich and used without further purification. HCl obtained from VWR was used for all the experiments. Colloidal rods were synthesized according to the procedure described in Ref. [37]. Briefly, 1 ml of HCl (0.05 M) was added to 4 ml of aqueous solution of $\text{FeCl}_3 \cdot 6\text{H}_2\text{O}$ (1 M). Fifteen milliliters of Milli-Q was added to the mixture to obtain a final volume of 20 ml. The solution was passed through 0.22 μm Millipore filters to remove any particulate contaminants and stored in a clean glass bottle with Teflon-lined screw cap. The glass bottle was tightly capped and placed in a preheated oven at 100 °C for 24 h. After aging, the samples were removed from the oven and quenched to room temperature under running tap water. The products were thoroughly cleaned using repeated cycles of centrifugation and dispersion in Milli-Q water.

B. Characterization and methods

The characterization of the shape and size of the colloidal rods was carried out using scanning electron microscopy

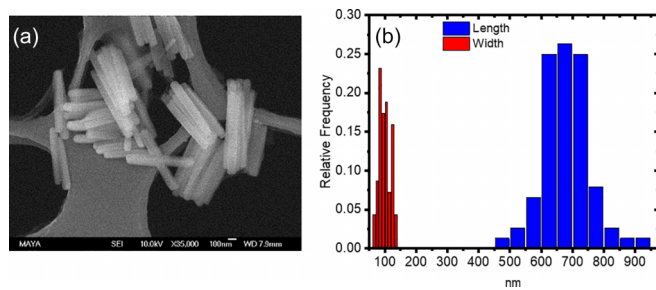


FIG. 1. (a) Representative SEM images for akaganeite-based colloidal rods of aspect ratios $\rho = 7.2$ and panel (b) represents the statistical distribution of length scales as has been obtained from panel (a).

(SEM) (ZEISS LEO Gemini 1560 and ZEISS Gemini 500 at an accelerating voltage of 15 kV). From the resulting transmission electron microscopic images, using ImageJ, the particle size distribution was determined by analyzing at least 100 particles. Figure 1(a) shows a representative micrograph of these rods, while panel (b) represents the statistical size analysis based on these images. The particle long and short axes were found to be $a = 676 \pm 75$ nm and $b = 93.5 \pm 14$ nm, respectively, leading to an aspect ratio of $\rho = 7.2$.

Multispeckle ultrasmall-angle x-ray photon correlation spectroscopy (UA-XPCS) was performed at the beam line ID02, ESRF, in a pinhole ultrasmall-angle x-ray scattering (USAXS) geometry. This unique instrument allows XPCS measurements on particle suspensions down to the μm^{-1} q (wave vector) range. The dispersions were filled in 1.0 mm glass capillaries. Experiments were performed using an X-ray of wavelength of 1.01 Å and a sample-to-detector distance of 30.55 m. The two-dimensional speckle patterns were recorded using an EIGER 500K pixel array detector [38]. The correlation functions were calculated using the Dynamix software package, developed at the ESRF. The time and ensemble averaged intensity-intensity autocorrelation functions were obtained by the azimuthal averaging of pixel corresponding to the same q using Dynamix package.

III. RESULTS AND DISCUSSION

Both DLS and XPCS measurements allow one to obtain the information about the particle dynamics on a length scale, which is on the order of $1/q$ via the intensity-intensity autocorrelation function,

$$g^{(2)}(\vec{q}, t) = \frac{\langle I(\vec{q}, \tau)I(\vec{q}, \tau + t) \rangle}{\langle I(\vec{q}) \rangle^2}, \quad (1)$$

where \vec{q} is the scattering vector with magnitude $q = 4\pi \sin(\theta/2)/\lambda$, θ being the scattering angle and λ being the wavelength in the scattering medium. Figure 2 represents the structural correlation and dynamics at the highest concentration studied, $\phi_{\text{max}} = 0.17$. Beyond this concentration, the system shows higher-order structures, such as nematic and smectic phases. Figure 2(a) shows the diffraction pattern in the form of a broad ring indicating an isotropic arrangement of the particles. Figure 2(b) represents the effective structure factor, which is obtained by dividing $I(q)/\phi$ by the normalized in-

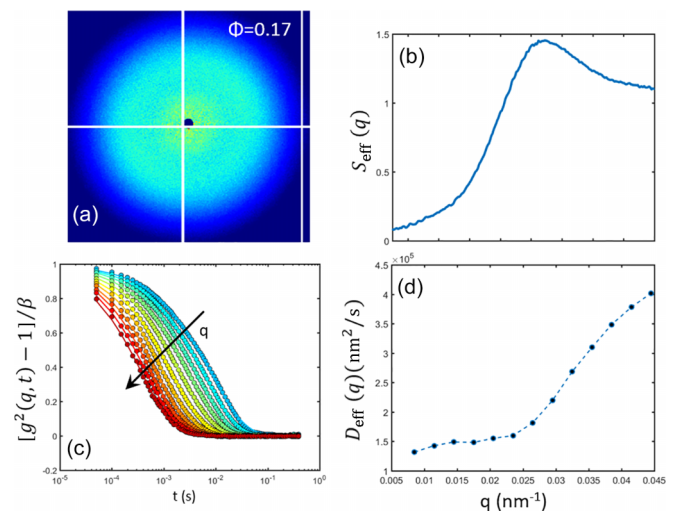


FIG. 2. (a) 2D scattering pattern and (b) effective structure factor for $\phi = 0.17$. (c) Intensity autocorrelation functions for different q values. The symbols represent the experimental data, while the line corresponds to the fit with KWW model. (d) Variation of D_{eff} as a function of q ; the black dots indicate the experimental data and the blue dashed line is a guide to the eye.

tensity of a very dilute sample of concentration $\phi_{\text{dil}} = 0.0028$; here, $I(q)$ is the radial intensity profile.

In principle, even for the monodisperse system, form and structure factors are coupled for rods and one cannot just divide the intensities to get structure factor. Polydispersity further complicates the situation and one should use decoupling approximation for a better result [39]. However, the decoupling approximation fails at these high aspect ratio. Further, as mentioned by Klein, when the polydispersity exceeds 5%, one cannot really compare the theoretical structure factor with the experimental one [40]. Nonetheless, as a first approximation, one can still use $S_{\text{eff}}(q) = \frac{I(q)/\phi}{I_{\text{dil}}(q)/\phi_{\text{dil}}}$.

For anisotropic particles such as rods, the interpretation of dynamic scattering data is intrinsically more complex than for spherical particles. In dynamic scattering experiments, the measured relaxation modes generally contain coupled contributions from translational and rotational diffusion, and the separation of these contributions is not straightforward, particularly at intermediate scattering vectors where both motions contribute simultaneously. In addition, polydispersity in rod length and diameter leads to a distribution of relaxation times, further complicating the extraction of well-defined dynamical parameters. At higher volume fractions, the situation becomes even more complex due to crowding, hydrodynamic interactions, and steric constraints, which modify both rotational and translational motion.

Figure 2(c) shows the intensity autocorrelation functions, $g^{(2)}(q, t)$, of the sample for different q values. The intermediate scattering function $g^{(1)}(\vec{q}, t)$ is related to $g^{(2)}(\vec{q}, t)$ via the Siegert relation, $g^{(1)}(\vec{q}, t) = \sqrt{[g^{(2)}(\vec{q}, t) - 1]/\beta}$, where β is the coherence factor of the experimental setup. $g^{(1)}(q, t)$ can be described phenomenologically by a Kohlrausch-Williams-Watts (KWW) expression,

$$g^{(1)}(q, t) = \exp[-(t/t_c)^\gamma], \quad (2)$$

where t_c is the relaxation time and γ is the KWW exponent that depends on the mechanism responsible for the relaxation of the density fluctuation. The average value of t_c is $\langle t_c \rangle = (t_c/\gamma)\Gamma(1/\gamma)$, where Γ is the Euler Gamma function [41]. For freely diffusing (Brownian motion) particles, $\gamma = 1$ and $\langle t_c \rangle = t_c$. In this case, the relaxation time is related to the diffusion constant D by $1/\langle t_c \rangle = Dq^2$. In principle, for any value of γ we can still define an effective diffusion coefficient, $D_{\text{eff}} = 1/(\langle t_c \rangle q^2)$, which is shown in Fig. 2(d) as a function of q for ϕ_{max} . One can observe that $1/D_{\text{eff}}(q)$ follows a similar trend with q as $S_{\text{eff}}(q)$ [Fig. 2(b)]. This particular behavior was first shown by De Gennes [42] and the mathematical expression for that is

$$D_{\text{eff}}(q)/D_0 = H_{\text{eff}}(q)/S_{\text{eff}}(q), \quad (3)$$

where D_0 is the free particle diffusion coefficient and $H_{\text{eff}}(q)$ is the effective hydrodynamic function.

The relaxation of density fluctuation at the nearest-neighbor length scale exhibits increasingly separated short- and long-time processes that are qualitatively described by local diffusion or rattling in the nearest-neighbor cage, followed by the opening of the cage and subsequent diffusion out of the cage, respectively. The timescale (t) for short-time diffusion is limited by $\tau_H \ll t \ll \tau_L$, where $\tau_H = R^2 \rho_{\text{sol}}/\eta_{\text{sol}}\phi$ and $\tau_L = R^2/D_0$ [30]. Here, R is the particle radius, ρ_{sol} is the solvent density, η_{sol} is the solvent viscosity. Given the size of our particles ($93.5 \times 676 \text{ nm}^2$), the limit of short-time diffusion in our case comes out to be $10^{-8} \text{ s} \ll t \ll 10^{-1} \text{ s}$. As our measurements were performed within the time window, $5 \times 10^{-5} \text{ s} \leq t \leq 10^{-1} \text{ s}$, our data are mainly dominated by the short-time relaxation processes with having some contributions from the long-time ones as well. For this system, we find that the variation of $1/D_{\text{eff}}(q)$ with q follows a trend that is similar to that followed by $S_{\text{eff}}(q)$ with q . Therefore, following Eq. (3) one can propose

$$D_{\text{eff}}(q)/D_0 = A_{\text{eff}}(q)/S_{\text{eff}}(q), \quad (4)$$

where $A_{\text{eff}}(q)$ is defined as the *effective amplitude function*. Similar behavior has been observed for colloidal ellipsoids as well [15,16]. The majority of the studies in the literature have demonstrated that the short-time diffusion coefficient follows $1/S_{\text{eff}}(q)$ behavior, whereas only a handful of them report about a similar scaling behavior for long-time diffusion coefficient for both hard sphere and screened Coulomb interactions [31,43,44]. Banchio *et al.* [44] have used simulations along with mode coupling theory and experiments to show the same scaling behavior for long-time diffusion coefficient with $1/S_{\text{eff}}(q)$ as for short-time ones. To the best of our knowledge, at present there is a lack of both theoretical and simulation studies that can account for this kind of scaling behavior for anisotropic particles.

Similar 2D scattering patterns indicating isotropic arrangement of particles has been observed for all concentrations studied. Figures 3(a) and 3(b) represent the effective structure factor and the corresponding dynamics at different concentrations, respectively; different colors correspond to different concentrations. One can observe that as ϕ increases, the structural correlation builds up; not only the relative height of the structure factor peak increases but also its width decreases as a function of increasing ϕ [Fig. 3(a)] indicating an increase in

the range of translational order. Figure 3(b), which shows the variation of $1/D_{\text{eff}}(q)$ as a function of ϕ , indicates not only De Gennes narrowing but also the slowing down of the system with increasing ϕ as expected due to the crowding effect. Experimentally, similar behavior has also been reported for spherical colloidal systems as well as for globular proteins, polymers, and flexible rods [30–35].

In principle, having measured $S_{\text{eff}}(q)$ and $D_{\text{eff}}(q)$ one can now extract $A_{\text{eff}}(q)$ [by using eq. (4)], shown in Fig. 3(c) for different concentrations. In order to calculate $A_{\text{eff}}(q)$, we have used $D_0 = 1.29 \times 10^6 \text{ nm}^2/\text{s}$, measured at $\phi_{\text{dil}} = 0.0028$. One can see that $A_{\text{eff}}(q)$ also exhibit a strong q dependence and follows a trend similar to $S_{\text{eff}}(q)$. Further, if dynamic scaling is also valid for our rods with $A_{\text{eff}}(q)$ and $H_{\text{eff}}(q)$ being related by a multiplicative constant [31], then one can expect similar behavior for $H_{\text{eff}}(q)$ for this anisotropic system as well. Although there are reports in the literature on the theoretical and experimental studies on $H_{\text{eff}}(q)$ for the hard and charged sphere systems [22,45,46], to the best of our knowledge there is no such experimental study on anisotropic particles, except our own for colloidal ellipsoids [15,16].

From the fitting of the correlation functions, it can be observed that the stretching exponent, γ , in Eq. (2) also changes with concentration. For the lowest concentration, γ is above 0.9 indicating a polydispersity contribution on the shape of the correlation functions. With increasing concentration in the liquid regime, γ gets smaller to a value of about 0.65 at the highest concentration. Similar behavior has been reported for anisotropic platelet and ellipsoid systems [13,15,16]. With increasing ϕ , the system approaches a kinetic arrest, as can be seen from Fig. 4. We have fitted our experimental data with (modified) Vogel-Fulcher-Tammann (VFT) expression, which is usually used to describe the increase in viscosity of glass-forming molecular liquids with decreasing temperature. However, in the modified expression, temperature is replaced by $1/\phi$, because for the colloidal dispersions ϕ plays a similar role as the temperature does for molecular glasses. Further, for colloids, modified VFT law is usually applied to describe the rise in the viscosity with ϕ and its dramatic increase at $\phi = \phi_m$ [47,48]. In our case, we have modified it further by replacing η_{sol}/η_0 , where η_{sol} and η_0 are the viscosity of the solvent and the zero shear viscosity of the system, respectively, with $D_{\text{eff}}(q_m)/D_0$ to obtain a mathematical expression:

$$D_{\text{eff}}(q_m)/D_0 = \exp\left(\frac{F\phi}{\phi_m - \phi}\right), \quad (5)$$

q_m being the q value corresponding to the structure factor peak. The fit of Eq. (5) can be seen in Fig. 4 as a solid line, where we found ϕ_m to be 0.23.

To place our results in the context of packing constraints and possible dynamical arrest, we consider the dense packing limit for rodlike particles established by Philipse [49], who showed using a random contact model that for sufficiently long rods ($L/D \geq 15$) the random closed-packed packing fraction scales approximately as $\phi_{\text{RCP}}(L/D) \approx c$, where $c \approx 5.4$ corresponds to the average number of contacts per particle. For shorter rods, however, deviations from this scaling are observed and no general predictive theory for the close-packed density exists. The rods used in the present work have $L/D \approx 7.2$ and therefore fall outside the regime where the

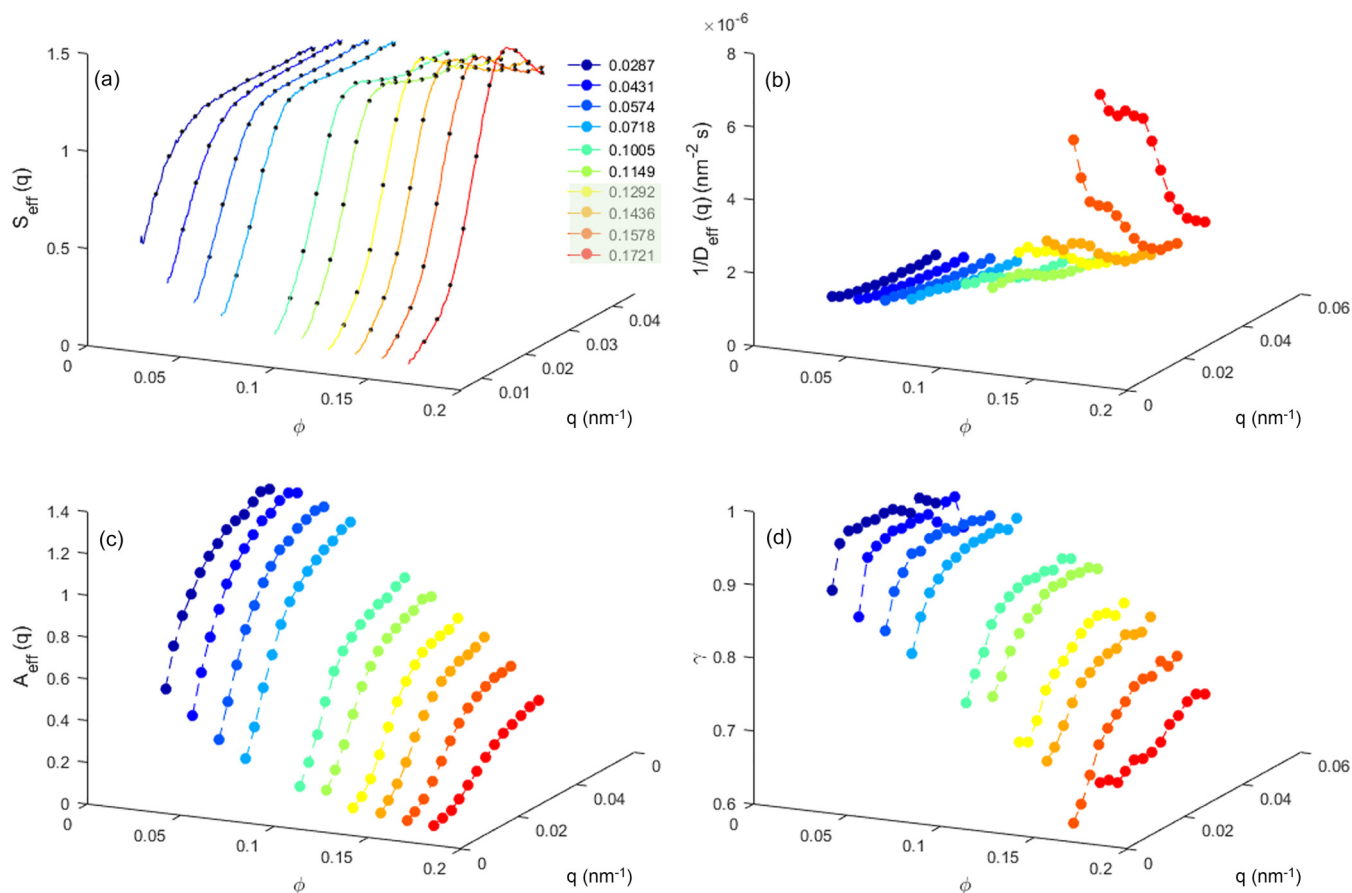


FIG. 3. (a) Variation of the structure factor $S_{\text{eff}}(q)$ as a function of q . The solid lines represent the experimental data, while the symbols indicate the q values at which the dynamics has been measured. (b) Variation of $1/D_{\text{eff}}(q)$ as a function of q . (c) Variation of the amplitude function $A_{\text{eff}}(q)$ as a function of q . (d) Variation of the exponent γ as a function of q . For panels (b)–(d), the symbols indicate the experimental data, while the solid lines are guide to the eye. For panels (a)–(d), different colors correspond to different volume fractions ϕ , which has been mentioned in the legend of panel (a).

asymptotic scaling is expected to hold. By interpolating the experimental data reported by Philipse, we estimate a random close-packing fraction of approximately $\phi_{\text{RCP}} \approx 0.37$ for rods

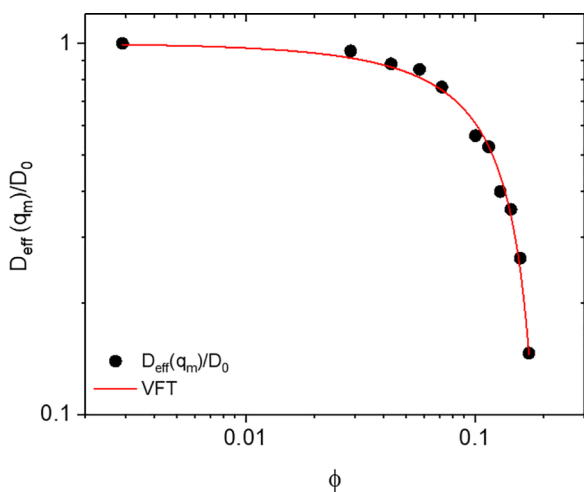


FIG. 4. Variation of the normalized diffusion coefficient $D_{\text{eff}}(q_m)/D_0$ with ϕ ; the symbols represent the experimental data, while the solid line indicates the fit with modified VFT law.

with this aspect ratio. This value can be compared with the concentration obtained from the VFT fit to the diffusion coefficient ($\phi_m = 0.23$). The lower value of ϕ_m indicates that dynamical arrest sets in well before the system reaches its geometric packing limit. A comparable separation between the glass transition and random close packing is observed for hard spheres, where the glass transition ($\phi_g \approx 0.58$) precedes the random close-packed density ($\phi_{\text{RCP}} \approx 0.64$). Our results suggest a similar distinction between dynamical arrest and geometric packing constraints in anisotropic rodlike particles. Further, we do not observe complete arrest of D_{eff} within the experimentally accessible concentration range, although a pronounced slowing down is observed. Interestingly, the extrapolated VFT divergence concentration was found to be slightly above the onset of nematic ordering in our system ($\phi \approx 0.22$), suggesting that any potential arrest would occur within an orientationally ordered phase rather than in an isotropic phase. In rodlike systems, orientational degrees of freedom are known to slow down more rapidly than translational motion, which can lead to orientationally arrested states such as orientational glasses [50,51] or freezing of nematic domains [2], as reported for ellipsoidal and rodlike particles, as well as for charged rod suspensions. Within this framework, we interpret the VFT extrapolation as indicating a tendency

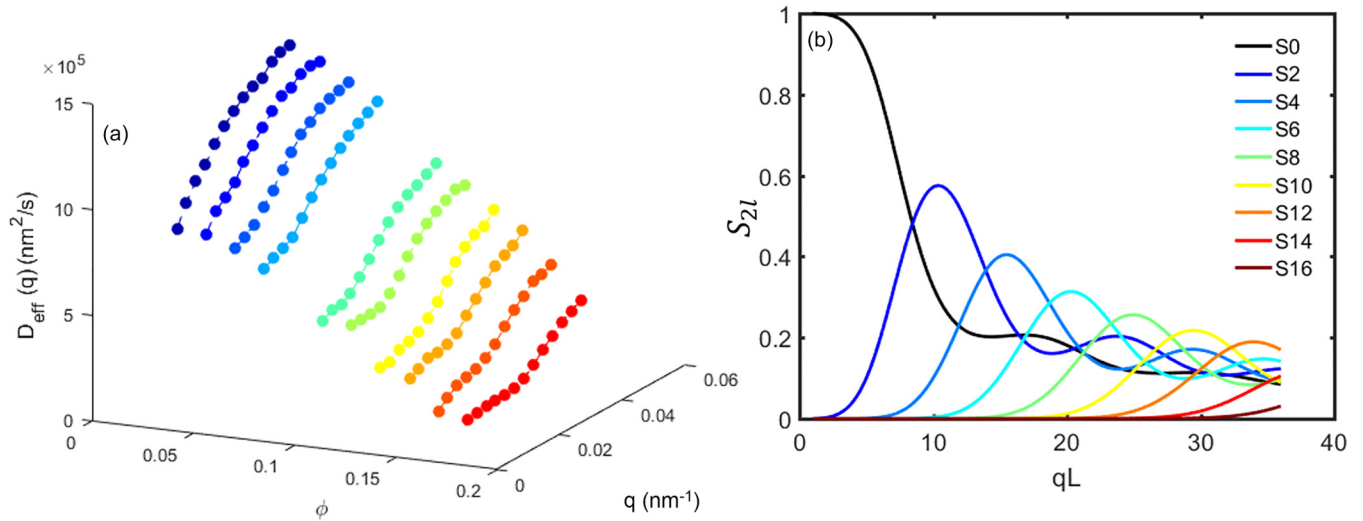


FIG. 5. (a) Variation of $D_{\text{eff}}(q)$ as a function of q . Different colors corresponds to different ϕ as mentioned in Fig. 3. (b) The expansion coefficients S_{2l} as functions of qL .

toward orientational or domain-level dynamical arrest rather than complete single-particle translational arrest.

Since the aspect ratio of the system under study is moderately large, $\rho = 7.2$, $D_{\text{eff}}(q)$ [shown in Fig. 5(a)] contains contributions from translational and rotational motions. As a result, the next natural question at hand to answer is that whether it is possible to split the contributions from these two aforementioned processes. For infinitely thin rods at infinite dilution, the intermediate scattering function $g^{(1)}(q, t)$ can be expressed as [36]

$$g^{(1)}(q, t) = \exp[-D_t q^2 t] \sum_{l=0}^{\infty} \exp[-D_r l(l+1)t] S_l(qL), \quad (6)$$

where S_l can be represented as

$$S_{2l}(qL) = \frac{(4l+1)}{2} \frac{[\int_{-1}^1 dx P_{2l}(x) j_0(\frac{1}{2}Lqx)]^2}{\int_{-1}^1 dx j_0^2(\frac{1}{2}Lqx)}, \quad (7)$$

$$S_{2l+1}(qL) = 0,$$

with P_l being the l th-order Legendre polynomial and j_0 being the Bessel function of first kind. Figure 5(b) shows the variation of S_{2l} as a function of qL . As one can find from Fig. 5(b), a significant contribution from rotational diffusion can be observed only when $qL > 5$.

Using Eqs. (6) and (7), one can fit the experimentally obtained correlation functions to get D_t and D_r up to a concentration $\phi = 0.115$, beyond which the applicability of this model breaks down and the correlation functions cannot be fitted anymore with it. For colloidal rods, in the noninteracting limit, three concentration regimes [52] have been defined, namely, dilute, semidilute, and concentrated regimes. For $\phi \ll 1/\rho^2$, the rods are under dilute condition and they rarely interact. In the semidilute range, $1/\rho^2 \ll \phi \ll 1/\rho$, each rod has few structural contacts with its neighbors but suspension Brownian dynamics are a strong function of number density. This strong dependence arises because particle rotations are hindered as a consequence of the fact that the mean separation between rods is less than the rod's length. Finally, in

the isotropic concentrated regime, $\phi \gg 1/\rho$, rod rotation is severely hindered by strong structural correlations and multiple, random inter-rod contacts. For $\rho = 7.2$, the semidilute range is defined as $0.0193 \ll \phi \ll 0.14$, and surprisingly the formalism developed by Dhont [36] breaks down as soon as ϕ approaches concentrated regime.

Figure 6(a) has shown one such fit for $\phi = 0.115$. The values of D_t and D_r obtained for different ϕ are shown in Figs. 6(b) and 6(c), respectively. At all the concentrations, D_t show minima at q values, which correspond to peak positions in the structure factors, which is indicative of the De Gennes narrowing behavior. From Fig. 6(c), one can observe an increase of D_r as a function of q at low q . However, all the reported studies of D_r are based on noninteracting systems where it is found that the behavior of D_r is q independent. Further, the formalism followed here to calculate the value of D_t and D_r is based on the assumptions that the system should consist of infinitely thin noninteracting rods, which is clearly not the scenario for our system. As a result, at this point we cannot come to a definitive conclusion about the upturn of D_r at low q .

IV. CONCLUSION

We have studied the dynamics at the nearest-neighbor length scale of colloidal rods over a broad concentration range in the isotropic phase by exploiting the ultrasmall-angle XPCS. Although the literature is replete with phase behavior and rheological properties for various rodlike systems, there has been an almost complete lack of experimental information about the relation between the structural correlation and the dynamical behavior. It is for this reason that we have performed a systematic study of the structural and dynamic properties of a model rod system using XPCS. With this study, we have not only shown the relation between the self-assembled structure and dynamics at the nearest-neighbor length scale in the isotropic phase but also experimentally determined the amplitude function. Further, we have experimentally

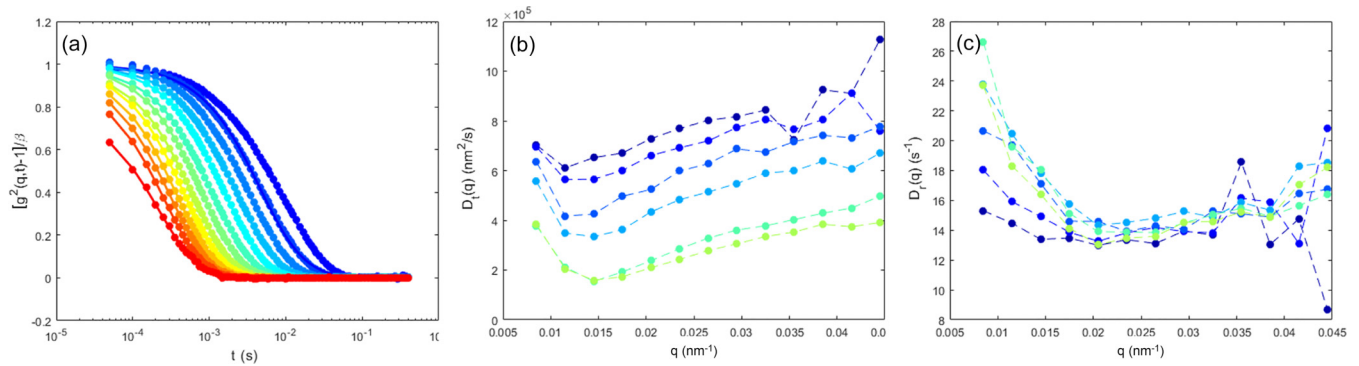


FIG. 6. (a) Intensity autocorrelation functions for different q values at $\phi = 0.115$. The symbols represent the experimental data, while the line corresponds to the fit with Eqs. (6) and (7); panels (b) and (c) represent the variation of D_t and D_r as a function of q . Different colors correspond to different ϕ as mentioned in Fig. 3.

determined the volume fraction corresponding to the arrest transition for colloidal rods of $\rho = 7.2$.

Finally, we have also tried to find out the contributions from D_t and D_r . While the behavior of D_t as a function of q is found to be quite convincing, D_r shows an upturn at low q . However, the model we have used to find out D_t and D_r is not optimal. One option to get a conclusive answer would be to develop a suitable theory considering the finite thickness of the rods under interacting conditions. The other option would be to measure similar system using polarized differential dynamic microscopy, where the contribution from D_t and D_r can be directly measured using depolarized technique [53].

Until recently, such an endeavor where one can explore the dynamics of a dense system near glass transition would have been perceived as very difficult experimentally due to a lack of available model systems when using the traditional experimental tools such as DLS or confocal microscopy. However, our study has shown that the type of anisotropic systems that can be used to study the colloidal glass transition can now be greatly extended, as turbidity becomes a minor issue when using XPCS. This opens avenues for exploring the dynamics of strongly interacting colloidal systems with a large variety of shapes and chemical compositions. We believe that our results will inspire future experimental studies on concentrated anisotropic particles. Further, we also believe that the

unsolved part of our quest regarding the contributions from D_t and D_r would motivate theoreticians to develop suitable theory for anisotropic systems.

ACKNOWLEDGMENTS

Peter Schurtenberger is acknowledged for providing support and Daniel Madsen is acknowledged for helping with the SEM measurement. Peter Holmqvist and Theyencheri Narayanan are acknowledged for many helpful discussions. Financial support from the Röntgen-Ångström Cluster Grant No. 2019-06075 and European Union's Horizon 2020 research and innovation program through the European Soft Matter Infrastructure grant (731019-EUSMI) are gratefully acknowledged. ESRF is acknowledged for granting beam time (SC-5054).

DATA AVAILABILITY

The data that support the findings of this article are not publicly available upon publication because it is not technically feasible and/or the cost of preparing, depositing, and hosting the data would be prohibitive within the terms of this research project. The data are available from the authors upon reasonable request.

- [1] I. Teraoka, N. Ookubo, and R. Hayakawa, Molecular theory on the entanglement effect of rodlike polymers, *Phys. Rev. Lett.* **55**, 2712 (1985).
- [2] K. Kang and J. K. G. Dhont, Glass transition in suspensions of charged rods: Structural arrest and texture dynamics, *Phys. Rev. Lett.* **110**, 015901 (2013).
- [3] C. K. Mishra, A. Rangarajan, and R. Ganapathy, Two-step glass transition induced by attractive interactions in quasi-two-dimensional suspensions of ellipsoidal particles, *Phys. Rev. Lett.* **110**, 188301 (2013).
- [4] Z. Zheng, R. Ni, F. Wang, M. Dijkstra, Y. Wang, and Y. Han, Structural signatures of dynamic heterogeneities in monolayers of colloidal ellipsoids, *Nat. Commun.* **5**, 3829 (2014).
- [5] Z. Zheng and Y. Han, Self-diffusion in two-dimensional hard ellipsoid suspensions, *J. Chem. Phys.* **133**, 124509 (2010).
- [6] Z. Zheng, F. Wang, and Y. Han, Glass transitions in quasi-two-dimensional suspensions of colloidal ellipsoids, *Phys. Rev. Lett.* **107**, 065702 (2011).
- [7] S. G. J. M. Kluijtmans, G. H. Koenderink, and A. P. Philipse, Self-diffusion and sedimentation of tracer spheres in (semi) dilute dispersions of rigid colloidal rods, *Phys. Rev. E* **61**, 626 (2000).
- [8] D. Mukhija and M. J. Solomon, Translational and rotational dynamics of colloidal rods by direct visualization with confocal microscopy, *J. Colloid Interface Sci.* **314**, 98 (2007).
- [9] D. Lehner, H. Lindner, and O. Glatter, Determination of the translational and rotational diffusion coefficients of rodlike par-

- ticles using depolarized dynamic light scattering, *Langmuir* **16**, 1689 (2000).
- [10] J. Rodríguez-Fernández, J. Pérez-Juste, L. M. Liz-Marzán, and P. R. Lang, Dynamic light scattering of short Au rods with low aspect ratios, *J. Phys. Chem. C* **111**, 5020 (2007).
- [11] I. Martchenko, H. Dietsch, C. Moitzi, and P. Schurtenberger, Hydrodynamic properties of magnetic nanoparticles with tunable shape anisotropy: Prediction and experimental verification, *J. Phys. Chem. B* **115**, 14838 (2011).
- [12] A. M. Shetty, G. M. Wilkins, J. Nanda, and M. J. Solomon, Multiangle depolarized dynamic light scattering of short functionalized single-walled carbon nanotubes, *J. Phys. Chem. C* **113**, 7129 (2009).
- [13] D. Kleshchanok, M. Heinen, G. Nägele, and P. Holmqvist, Dynamics of charged gibbsite platelets in the isotropic phase, *Soft Matter* **8**, 1584 (2012).
- [14] A. Pal, V. A. Martinez, T. H. Ito, J. Arlt, J. J. Crassous, W. C. Poon, and P. Schurtenberger, Anisotropic dynamics and kinetic arrest of dense colloidal ellipsoids in the presence of an external field studied by differential dynamic microscopy, *Sci. Adv.* **6**, eaaw9733 (2020).
- [15] A. Pal, M. A. Kamal, and P. Schurtenberger, Structure and anisotropic dynamics of stimuli responsive colloidal ellipsoids at the nearest neighbor length scale, *J. Colloid Interface Sci.* **621**, 352 (2022).
- [16] A. Pal, M. A. Kamal, P. Holmqvist, and P. Schurtenberger, Structure and dynamics of dense colloidal ellipsoids at the nearest-neighbor length scale, *Phys. Rev. Res.* **3**, 023254 (2021).
- [17] T. Hoshino, M. Nakayama, S. Fujinami, T. Nakatani, Y. Kohmura, and T. Kato, Static structure and dynamical behavior of colloidal liquid crystals consisting of hydroxyapatite-based nanorod hybrids, *Soft Matter* **15**, 3315 (2019).
- [18] M. J. Solomon and P. T. Spicer, Microstructural regimes of colloidal rod suspensions, gels, and glasses, *Soft Matter* **6**, 1391 (2010).
- [19] S. Abakumov, O. Deschaume, C. Bartic, C. Lang, O. Korculanin, J. K. G. Dhont, and M. P. Lettinga, Uncovering log jamming in semidilute suspensions of quasi-ideal rods, *Macromolecules* **54**, 9609 (2021).
- [20] A. Pal, T. Zinn, M. A. Kamal, T. Narayanan, and P. Schurtenberger, Anomalous dynamics of magnetic anisotropic colloids studied by XPCS, *Small* **14**, 1802233 (2018).
- [21] A. Pal, M. A. Kamal, T. Zinn, J. K. G. Dhont, and P. Schurtenberger, Anisotropic dynamics of magnetic colloidal cubes studied by X-ray photon correlation spectroscopy, *Phys. Rev. Mater.* **5**, 035603 (2021).
- [22] A. J. Banchio, J. Gapinski, A. Patkowski, W. Häußler, A. Fluerasu, S. Sacanna, P. Holmqvist, G. Meier, M. P. Lettinga, and G. Nägele, Many-body hydrodynamic interactions in charge-stabilized suspensions, *Phys. Rev. Lett.* **96**, 138303 (2006).
- [23] A. Robert, E. Wandersman, E. Dubois, V. Dupuis, and R. Perzynski, Glassy dynamics and aging in a dense ferrofluid, *Europhys. Lett.* **75**, 764 (2006).
- [24] T. Zinn, L. Sharpnack, and T. Narayanan, Dynamics of magnetic Janus colloids studied by ultra small-angle X-ray photon correlation spectroscopy, *Soft Matter* **19**, 2311 (2023).
- [25] T. Hoshino, M. Nakayama, Y. Hosokawa, K. Mochizuki, S. Kajiyama, Y. Kohmura, and T. Kato, Experimental probing of dynamic self-organized columnar assemblies in colloidal liquid crystals, *Nanoscale Adv.* **5**, 3646 (2023).
- [26] Y. Chushkin, A. Gulotta, F. Roosen-Runge, A. Pal, A. Stradner, and P. Schurtenberger, Probing cage relaxation in concentrated protein solutions by X-ray photon correlation spectroscopy, *Phys. Rev. Lett.* **129**, 238001 (2022).
- [27] C. Graf, M. Deggelmann, M. Hagenbüchle, H. Kramer, R. Krause, C. Martin, and R. Weber, Dynamic light scattering by aqueous solutions of rodlike fd-virus particles, *J. Chem. Phys.* **95**, 6284 (1991).
- [28] P. Holmqvist, V. Meester, F. Westermeier, and D. Kleshchanok, Rotational diffusion in concentrated platelet systems measured with X-ray photon correlation spectroscopy, *J. Chem. Phys.* **139**, 084905 (2013).
- [29] M. A. Kamal, M. Brizioli, T. Zinn, T. Narayanan, R. Cerbino, F. Giavazzi, and A. Pal, Dynamics of anisotropic colloidal systems: What to choose, DLS, DDM or XPCS?, *J. Colloid Interface Sci.* **660**, 314 (2024).
- [30] A. J. Banchio and G. Nägele, Short-time transport properties in dense suspensions: From neutral to charge-stabilized colloidal spheres, *J. Chem. Phys.* **128**, 104903 (2008).
- [31] P. N. Segrè and P. N. Pusey, Scaling of the dynamic scattering function of concentrated colloidal suspensions, *Phys. Rev. Lett.* **77**, 771 (1996).
- [32] W. van Meegen, R. Ottewill, S. Owens, and P. N. Pusey, Measurement of the wave-vector dependent diffusion coefficient in concentrated particle dispersions, *J. Chem. Phys.* **82**, 508 (1985).
- [33] B. M. Fine, A. Lomakin, O. O. Ogun, and G. B. Benedek, Static structure factor and collective diffusion of globular proteins in concentrated aqueous solution, *J. Chem. Phys.* **104**, 326 (1996).
- [34] M. Adam and M. Delsanti, Dynamical properties of polymer solutions in good solvent by Rayleigh scattering experiments, *Macromolecules* **10**, 1229 (1977).
- [35] U. Zettl, S. T. Hoffmann, F. Koberling, G. Krausch, J. Enderlein, L. Harnau, and M. Ballauff, Self-diffusion and cooperative diffusion in semidilute polymer solutions as measured by fluorescence correlation spectroscopy, *Macromolecules* **42**, 9537 (2009).
- [36] J. K. G. Dhont, *An Introduction to Dynamics of Colloids* (Elsevier, 1996), Vol. 2.
- [37] E. Matijević and P. Scheiner, Ferric hydrous oxide sols: III. Preparation of uniform particles by hydrolysis of Fe (III)-chloride, -nitrate, and -perchlorate solutions, *J. Colloid Interface Sci.* **63**, 509 (1978).
- [38] T. Zinn, A. Homs, L. Sharpnack, G. Tinti, E. Fröjdh, P.-A. Douissard, M. Kocsis, J. Möller, Y. Chushkin, and T. Narayanan, Ultra-small-angle X-ray photon correlation spectroscopy using the Eiger detector, *J. Synchrotron Radiat.* **25**, 1753 (2018).
- [39] M. Kotlarchyk and S.-H. Chen, Analysis of small angle neutron scattering spectra from polydisperse interacting colloids, *J. Chem. Phys.* **79**, 2461 (1983).
- [40] W. Brown (ed.), *Light Scattering: Principles and Development*, Monographs on the Physics and Chemistry of Materials, Vol. 53 (Clarendon Press, Oxford, 1996).
- [41] C. Lindsey and G. Patterson, Detailed comparison of the Williams–Watts and Cole–Davidson functions, *J. Chem. Phys.* **73**, 3348 (1980).

- [42] P. G. De Gennes, Liquid dynamics and inelastic scattering of neutrons, *Physica* **25**, 825 (1959).
- [43] P. Holmqvist and G. Nägele, Long-time dynamics of concentrated charge-stabilized colloids, *Phys. Rev. Lett.* **104**, 058301 (2010).
- [44] A. J. Banchio, M. Heinen, P. Holmqvist, and G. Nägele, Short- and long-time diffusion and dynamic scaling in suspensions of charged colloidal particles, *J. Chem. Phys.* **148**, 134902 (2018).
- [45] J. Riest, T. Eckert, W. Richtering, and G. Nägele, Dynamics of suspensions of hydrodynamically structured particles: Analytic theory and applications to experiments, *Soft Matter* **11**, 2821 (2015).
- [46] J. Gapinski, A. Patkowski, A. Banchio, J. Buitenhuis, P. Holmqvist, M. Lettinga, G. Meier, and G. Nägele, Structure and short-time dynamics in suspensions of charged silica spheres in the entire fluid regime, *J. Chem. Phys.* **130**, 084503 (2009).
- [47] G. Brambilla, D. El Masri, M. Pierno, L. Berthier, L. Cipelletti, G. Petekidis, and A. B. Schofield, Probing the equilibrium dynamics of colloidal hard spheres above the mode-coupling glass transition, *Phys. Rev. Lett.* **102**, 085703 (2009).
- [48] J. Mattsson, H. M. Wyss, A. Fernandez-Nieves, K. Miyazaki, Z. Hu, D. R. Reichman, and D. A. Weitz, Soft colloids make strong glasses, *Nature (London)* **462**, 83 (2009).
- [49] A. P. Philipse, The random contact equation and its implications for (colloidal) rods in packings, suspensions, and anisotropic powders, *Langmuir* **12**, 1127 (1996).
- [50] J. Roller, A. Laganapan, J.-M. Meijer, M. Fuchs, and A. Zumbusch, Observation of liquid glass in suspensions of ellipsoidal colloids, *Proc. Natl. Acad. Sci. USA* **118**, e2018072118 (2021).
- [51] H. Wang, Z. Zhang, and X. S. Ling, 2D phase behaviors of colloidal ellipsoids and rods, *Front. Phys.* **10**, 1043983 (2022).
- [52] M. Doi and S. Edwards, *The Theory of Polymer Dynamics* (Clarendon Press, Oxford, 1986).
- [53] F. Giavazzi, C. Haro-Pérez, and R. Cerbino, Simultaneous characterization of rotational and translational diffusion of optically anisotropic particles by optical microscopy, *J. Phys.: Condens. Matter* **28**, 195201 (2016).